


Suppression of $\Lambda(1520)$ resonance production in central Pb-Pb collisions at $\sqrt{s_{NN}} = 2.76$ TeVS. Acharya *et al.**
(ALICE Collaboration) (Received 31 May 2018; revised manuscript received 19 September 2018; published 8 February 2019)

The production yield of the $\Lambda(1520)$ baryon resonance is measured at midrapidity in Pb-Pb collisions at $\sqrt{s_{NN}} = 2.76$ TeV with the ALICE detector at the Large Hadron Collider (LHC). The measurement is performed in the $\Lambda(1520) \rightarrow pK^-$ (and charge conjugate) hadronic decay channel as a function of the transverse momentum (p_T) and collision centrality. The ratio of the p_T -integrated production of $\Lambda(1520)$ baryons relative to Λ baryons in central collisions is suppressed by about a factor of 2 with respect to peripheral collisions. This is the first observation of the suppression of a baryonic resonance at the LHC and the first 3σ evidence of $\Lambda(1520)$ suppression within a single collision system. The measured $\Lambda(1520)/\Lambda$ ratio in central collisions is smaller than the value predicted by the statistical hadronization model calculations. The shape of the measured p_T distribution and the centrality dependence of the suppression are reproduced by the EPOS3 Monte Carlo event generator. The measurement adds further support to the formation of a dense hadronic phase in the final stages of the evolution of the fireball created in heavy-ion collisions, lasting long enough to cause a significant reduction in the observable yield of short-lived resonances.

DOI: [10.1103/PhysRevC.99.024905](https://doi.org/10.1103/PhysRevC.99.024905)**I. INTRODUCTION**

High-energy heavy-ion collisions provide an excellent means to study the properties of nuclear matter under extreme conditions and the phase transition to a deconfined state of quarks and gluons (quark-gluon plasma, QGP [1]) predicted by lattice QCD calculations [2]. The bulk properties of the matter created in high-energy nuclear reactions have been widely studied at the Relativistic Heavy Ion Collider (RHIC) and at the Large Hadron Collider (LHC) and are well described by hydrodynamic and statistical models. The initial hot and dense partonic matter rapidly expands and cools, eventually undergoing a transition from the QGP to a hadron gas phase [3]. The relative abundances of stable particles are consistent with chemical equilibrium and are successfully described by statistical hadronization models (SHMs) [4–6]. They are determined by the “chemical freeze-out” temperature T_{ch} and the baryochemical potential μ_B [4,7], reflecting the thermodynamic characteristics of the chemical freeze-out. In the final stage of the collision, a dense hadron gas is expected to form and to expand until the system eventually decouples when elastic interactions cease. Hadronic resonances with lifetimes shorter than or comparable to the timescale of the fireball evolution (a few fm/c) are sensitive probes of the dynamics and properties of the medium formed after hadronization [8]. Within the SHM,

they are expected to be produced with abundances consistent with the chemical equilibrium parameters T_{ch} and μ_B , but the measured yields might be modified after the chemical freeze-out by the hadronic phase. Because of their short lifetimes, resonances can decay within the hadronic medium, which can alter or destroy the correlation among the decay daughters via interactions (rescattering) with the surrounding hadrons, hence reducing the observed yield. Alternatively, an increase (regeneration) might also be possible due to resonance formation in the hadronic phase [9]. The observed yield of hadronic resonances depends on the resonance lifetime, the duration of the hadronic phase, and the relative scattering cross section of the decay daughters within the hadronic medium.

Recent results from the ALICE Collaboration in Pb-Pb collisions at $\sqrt{s_{NN}} = 2.76$ TeV [10] show that the production yields of the $K^*(892)^0$ resonance are suppressed in central collisions with respect to peripheral collisions and are overestimated by SHM predictions. This phenomenon might be due to the short $K^*(892)^0$ lifetime ($\tau \sim 4$ fm/c) and suggests the dominance of destructive rescattering over regeneration processes in the hadronic phase. No suppression is observed for the longer lived $\phi(1020)$ meson ($\tau \sim 46$ fm/c), indicating that it decays mostly outside the fireball. Both observations are in agreement with the calculations of EPOS3, a model that includes a microscopic description of the hadronic phase [11]. Within this model, the lifetime of the hadronic phase formed in central Pb-Pb collisions at $\sqrt{s_{NN}} = 2.76$ TeV is predicted to be ~ 10 fm/c. The measurement of the production of the $\Lambda(1520)$ baryonic resonance, owing to its characteristic lifetime ($\tau \sim 12.6$ fm/c), serves as an excellent probe to further constrain the formation, the evolution, and the characteristics of the hadronic phase.

In this article, we present the first measurement of $\Lambda(1520)$ production in Pb-Pb collisions at $\sqrt{s_{NN}} = 2.76$ TeV. The

*Full author list given at the end of the article.

Published by the American Physical Society under the terms of the [Creative Commons Attribution 4.0 International](https://creativecommons.org/licenses/by/4.0/) license. Further distribution of this work must maintain attribution to the author(s) and the published article's title, journal citation, and DOI.

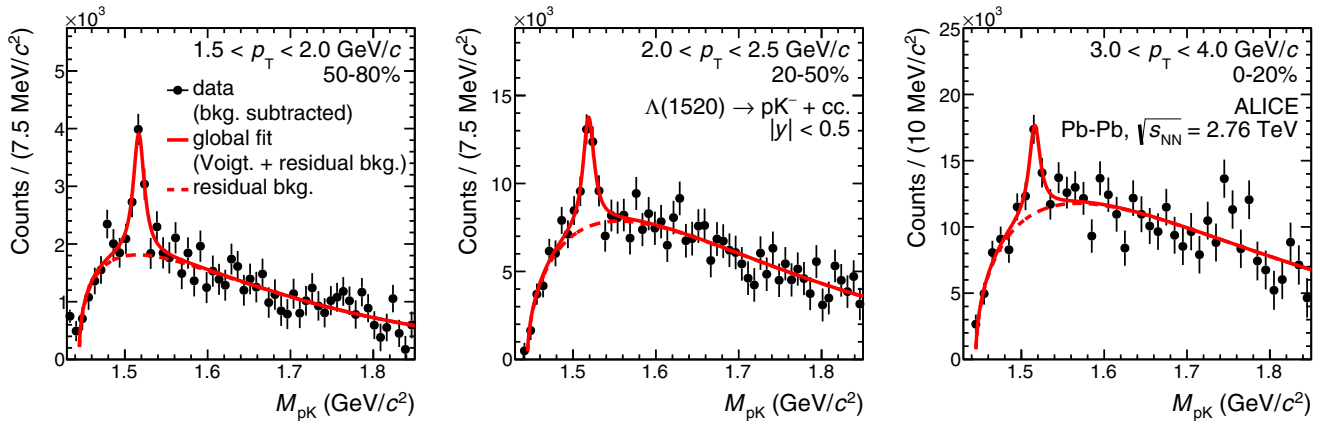


FIG. 1. Example invariant-mass distributions of the $\Lambda(1520) \rightarrow pK^-$ (and charged conjugate) reconstruction after subtraction of the mixed-event background. The solid line represents the global fit (signal + residual background) to the data while the dashed line indicates the estimated residual background. The error bars indicate the statistical uncertainties of the data.

measurement is performed at midrapidity, $|y| < 0.5$, with the ALICE detector [12] at the LHC and is based on an analysis of about 15 million minimum-bias Pb-Pb collisions recorded in 2010. Previous results on $\Lambda(1520)$ production in high-energy hadronic collisions have been reported by STAR in pp , d -Au, and Au-Au collisions at $\sqrt{s_{NN}} = 200$ GeV at RHIC [13,14].

II. EXPERIMENTAL SETUP AND DATA ANALYSIS

A detailed description of the ALICE experimental apparatus and its performance can be found in Ref. [15]. The relevant features of the main detectors utilized in this analysis are outlined here. The V0 detector is composed of two scintillator hodoscopes, placed on either side of the interaction point, and covers the pseudorapidity regions $2.8 < \eta < 5.1$ and $-3.7 < \eta < -1.7$, respectively. It is employed for triggering, background suppression, and collision-centralty determination. The inner tracking system (ITS) and the time-projection chamber (TPC) provide vertex reconstruction and charged-particle tracking in the central barrel, within a solenoidal magnetic field of 0.5 T. The ITS is a high-resolution tracker made of six cylindrical layers of silicon detectors. The TPC is a large cylindrical drift detector of radial and longitudinal dimensions of about $85 < r < 247$ cm and $-250 < z < 250$ cm, respectively. Charged-hadron identification is performed by the TPC via specific ionization energy loss (dE/dx) and by the time-of-flight (TOF) detector. The TOF is located at a radius of 370–399 cm and measures the particle time of flight with a resolution of about 80 ps, allowing hadron identification at higher momenta. A minimum-bias trigger was configured to select hadronic events with high efficiency, requiring a combination of hits in the two innermost layers of the ITS and in the V0 detector. The contamination from beam-induced background is removed offline, as discussed in detail in Refs. [16,17]. The collision centrality is determined based on the signal amplitude of the V0 detector, whose response is proportional to the event multiplicity. A complete description of the event selection and centrality determination can be found in Ref. [18].

The $\Lambda(1520)$ resonance is reconstructed via invariant-mass analysis of its decay daughters in the hadronic decay channel $\Lambda(1520) \rightarrow pK^-$ (and charge conjugate, c.c.), with a branching ratio of $22.5 \pm 0.5\%$ [19]. Particle and antiparticle states are combined to enhance the statistical significance of the reconstructed signal. $\Lambda(1520)$ refers to their sum in the following, unless otherwise specified. Candidate daughters are selected from tracks reconstructed by the ITS and TPC, are required to have $p_T > 150$ MeV/c, and are restricted to the pseudorapidity range $|\eta| < 0.8$ for uniform acceptance and efficiency performance. Furthermore, a cut on the impact parameter to the primary vertex is applied to reduce contamination from secondary tracks emanating from weak decays or from interactions with the detector material. Details on the track selection can be found in Ref. [10]. Kaons and protons are identified from the combined information of the track dE/dx in the TPC and the time of flight measured by the TOF. The invariant-mass distribution of unlike-sign pairs of selected kaon and proton tracks is constructed for each centrality class and p_T interval. The rapidity of the candidate $\Lambda(1520)$ is required to be within $|y| < 0.5$. A large source of background from random combinations of uncorrelated hadrons affects the invariant-mass spectrum. A mixed-event technique [20] is employed to estimate the combinatorial background, using unlike-sign proton and kaon tracks taken from different events with similar characteristics. The background is normalized and corrected for event-mixing distortions using a fit to the mixed/same-event ratio of like-sign pairs. Figure 1 shows examples of the reconstructed invariant-mass distribution after background subtraction. The $\Lambda(1520)$ raw yield is then extracted by means of a global fit, where a Voigtian function (the convolution of the nonrelativistic Breit-Wigner with the Gaussian detector resolution) is used to describe the signal. The shape of the residual background resembles that of a Maxwell-Boltzmann distribution; therefore the residual background is fitted with a similar functional form,

$$f_{\text{background}}(m_{pK}) = B \sqrt{(m_{pK} - m_{\text{cutoff}})^n} C^{3/2} \exp[-C(m_{pK} - m_{\text{cutoff}})^n], \quad (1)$$

TABLE I. Main contributions to the systematic uncertainty of the $\Lambda(1520)$ p_T -differential yield in 0–20%, 20–50%, and 50–80% centrality classes. The values are relative uncertainties (standard deviations expressed in %). When appropriate, they are reported for the lowest and highest measured p_T bin. The total systematic uncertainty and the contribution uncorrelated across centralities (after removing the common uncertainties) are also reported.

	0–20%	20–50%	50–80%
Signal extraction	12	11	9
Global tracking efficiency	10–10.5	10–10.5	10–10.5
TOF matching efficiency	1–6.5	1–6.5	0–6.5
Particle identification	3	3	3
Material and interactions	3.5–2.5	3.5–2.5	4.5–2.5
$\Lambda(1520)$ true p_T distribution	3.5–1	4.5–1	2.5–1
Normalization	0.5	1.5	4.5
Total	17–17.5	16.5–17	15.5–16.5
Uncorrelated	12–11.5	11.5–10.5	9.5–9.5

where B (normalization), m_{cutoff} (low-mass cutoff), C , and n are free parameters.

The raw yields are corrected for the decay branching fraction and for detector acceptance, reconstruction, track selection, and particle-identification efficiency, evaluated through a detailed Monte Carlo simulation of the ALICE detector. Simulation events are produced using the HIJING Monte Carlo event generator [21] with the addition of $\Lambda(1520)$ signals (particle and antiparticle states). Particle transport is performed by GEANT3 [22].

The main sources of systematic uncertainty on the corrected yields are summarized in Table I. They include the signal extraction procedures as well as the contributions related to the efficiency corrections (true p_T distribution of $\Lambda(1520)$, track selection, particle identification, material budget, and hadronic cross section) and event normalization. A significant fraction of this uncertainty, estimated to be about 12%, is common to all centrality classes.

III. RESULTS AND DISCUSSION

The fully corrected p_T -differential yields of $\Lambda(1520)$ measured in $|y| < 0.5$ are shown in Fig. 2 in the centrality classes 0–20%, 20–50%, and 50–80%. The spectral shapes are compared with predictions from the blast-wave model [23], which assumes particle production from thermal sources expanding with a common transverse velocity. The parameters of the model are the ones obtained from published results on pion, kaon, and proton production in Pb-Pb collisions [24]. The good agreement of the blast-wave predictions with the data is consistent with the scenario where $\Lambda(1520)$ undergoes a similar hydrodynamic evolution as pions, kaons, and protons with a common transverse expansion velocity that increases with centrality. The p_T distributions are also compared to predictions of the EPOS3 model [11], a Monte Carlo generator founded on parton-based Gribov-Regge theory, which describes the full evolution of a heavy-ion collision. The model employs viscous hydrodynamic calculations for the

description of the expansion of the bulk partonic matter. EPOS3 incorporates the UrQMD [25,26] transport model to describe the interactions among particles in the hadronic phase in a microscopic approach. The results from the model are in rather good agreement with the measured $\Lambda(1520)$ spectral shapes in all centrality classes, but the model overestimates the yields in central (0–20%) and semicentral (20–50%) collisions.

The p_T -integrated yield, dN/dy , and the average transverse momentum, $\langle p_T \rangle$, are computed by integrating the data and using extrapolations to estimate the yields in the unmeasured regions. The extrapolations are obtained using the best fit of the blast-wave function to the p_T distributions. Several other fit functions (Maxwell-Boltzmann, Fermi-Dirac, m_T exponential, p_T exponential) are employed to estimate the systematic uncertainties. The fraction of the yields in the extrapolated regions are 6.2%, 6.2%, and 10.4% for 0–20%, 20–50%, and 50–80% centrality events, respectively. The total dN/dy systematic uncertainties are 17.2%, 16.5%, and 15.6%, with a significant contribution common to all centrality classes of about 12%. The total systematic uncertainties on $\langle p_T \rangle$ are 6.9%, 7.2%, and 6.9%. The values of dN/dy and $\langle p_T \rangle$ for $\Lambda(1520)$ are reported in Table II.

The ratio of the p_T -integrated yield of $\Lambda(1520)$ to that of its stable counterpart, Λ , highlights the characteristics of resonance production directly related to the particle lifetime, as possible effects due to valence-quark composition cancel. The yields of Λ have been previously measured by ALICE in Pb-Pb collisions at $\sqrt{s_{NN}} = 2.76$ TeV [27]. Since the centrality classes for $\Lambda(1520)$ are different from those of the measured Λ yields, the latter has been interpolated from the measured values fitting their dependence on the number of participating nucleons in the collisions (N_{part}) with the empirical parametrization $a + b\langle N_{\text{part}} \rangle^c$, where a , b , and c are free parameters. Moreover, the $\bar{\Lambda}$ yield, which was not published in Ref. [27], has been assumed equal to that of Λ , as expected at LHC energies [24]. In the following, Λ refers to the sum of particle and antiparticle states, except for ALICE, where it is defined as 2Λ . The yield ratios $\Lambda(1520)/\Lambda$ are reported in Table II.

Figures 3 and 4, respectively, present the $\langle p_T \rangle$ of $\Lambda(1520)$ and the $\Lambda(1520)/\Lambda$ yield ratios as a function of the cubic root of the charged-particle multiplicity density at midrapidity [17], $(dN_{\text{ch}}/d\eta)^{1/3}$. The latter is used as a proxy for the system radius to emphasize the system-size dependence of $\Lambda(1520)$ production, as suggested by femtosopic studies using Bose-Einstein correlations [28]. The $\langle p_T \rangle$ increases significantly with increasing charged-particle multiplicity, hence with increasing collision centrality (Fig. 3). The value in central (0–20%) collisions is 23% higher than the one in peripheral (50–80%) collisions. The measured $\langle p_T \rangle$ is compared to the prediction from the blast-wave model discussed previously [23,24]. The good agreement confirms the consistency of the $\Lambda(1520)$ data with a common hydrodynamic evolution picture. The $\langle p_T \rangle$ results also highlight the good agreement with the prediction from the EPOS3 [11] model. It is noteworthy that EPOS3 fails to describe the data when the UrQMD transport stage is disabled, underlining the importance of

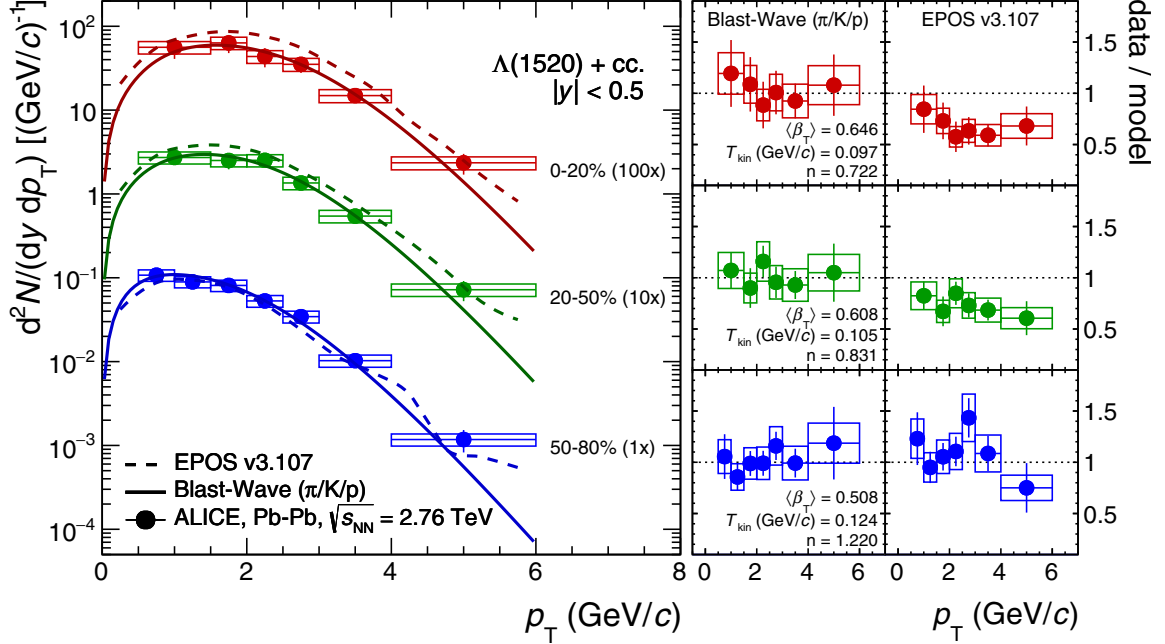


FIG. 2. (Left) p_T -differential yields of $\Lambda(1520)$ at midrapidity, $|y| < 0.5$, in the centrality classes 0–20%, 20–50%, and 50–80%. The solid and dashed curves represent predictions from the blast-wave model (normalization fitted to the data) and EPOS3, respectively. The horizontal error bars represents the width of the measured p_T interval. (Right) Ratio of the data to the blast-wave and EPOS3 predictions.

the latter in the description of the evolution of heavy-ion collisions.

A gradual decrease of the $\Lambda(1520)/\Lambda$ yield ratio with increasing charged-particle multiplicity is observed from peripheral to central Pb-Pb collisions (Fig. 4). The $\Lambda(1520)$ suppression in central Pb-Pb events with respect to peripheral events is measured as the double ratio

$$R_{cp}^{\Lambda^*/\Lambda} = \frac{[\Lambda(1520)/\Lambda]_{0-20\%}}{[\Lambda(1520)/\Lambda]_{50-80\%}} = 0.54 \pm 0.08(\text{stat}) \pm 0.12(\text{syst}), \quad (2)$$

where common uncertainties cancel. $\Lambda(1520)/\Lambda$ in central collisions is about 45% lower than in peripheral collisions. The result provides the first evidence for $\Lambda(1520)$ suppression in heavy-ion collisions, with a 3.1σ confidence level. The ratio is compared to grand-canonical equilibrium predictions from the GSI-Heidelberg [4], THERMUS [29], and SHARE3 [30] models, whose parameters have been determined from fits to stable particles [31]. The ratio is also compared to the nonequilibrium configuration implemented

in SHARE3, where the undersaturation (oversaturation) parameters γ_s (strange) and γ_q (light quarks) are free [32]. All models describe the yield of stable hadrons well. $\Lambda(1520)/\Lambda$ in central collisions is lower than SHM predictions by values ranging from 37% to 52%, depending on the reference model. Figure 4 also shows the data from the STAR Collaboration at RHIC in Au-Au, d -Au, and pp collisions at $\sqrt{s_{NN}} = 200$ GeV [13,14]. The trend of the suppression is similar to the one seen from STAR data in Au-Au collisions at $\sqrt{s_{NN}} = 200$ GeV. The current measurement of $\Lambda(1520)$ suppression has a higher precision at 3.1σ confidence level, as compared to the 1.8σ confidence level of STAR data in Au-Au collisions. Finally, the multiplicity dependence of the $\Lambda(1520)/\Lambda$ ratio is compared with the prediction from EPOS3 [11] (Fig. 4). It is important to note that the model, although it systematically overestimates the data, describes the trend of the suppression well. The double ratio $R_{cp}^{\Lambda^*/\Lambda}$ is in agreement with the data within the uncertainties, although the model is about 25% higher. This might hint to a longer lifetime of the hadronic phase than the value obtained from EPOS3 calculations ($\tau_{\text{hadr}} \sim 8.5$ fm/c) or to an imprecise description

TABLE II. $\Lambda(1520)$ integrated yields, p_T -integrated ratio of $\Lambda(1520)/\Lambda$, $\langle p_T \rangle$ of $\Lambda(1520)$ production and corresponding uncertainties in 0–20%, 20–50%, and 50–80% centrality classes. The first and second uncertainties indicate the statistical and total systematic error, respectively. The values in parentheses show the systematic uncertainty excluding the contributions common to all centrality classes.

	dN/dy	$\Lambda(1520)/\Lambda$	$\langle p_T \rangle$ (GeV/c)
0–20%	$1.56 \pm 0.20 \pm 0.27$ (0.19)	$0.038 \pm 0.005 \pm 0.008$ (0.006)	$1.85 \pm 0.09 \pm 0.13$ (0.10)
20–50%	$0.70 \pm 0.06 \pm 0.12$ (0.08)	$0.044 \pm 0.004 \pm 0.009$ (0.007)	$1.76 \pm 0.06 \pm 0.13$ (0.11)
50–80%	$0.22 \pm 0.02 \pm 0.03$ (0.02)	$0.069 \pm 0.006 \pm 0.013$ (0.010)	$1.50 \pm 0.05 \pm 0.10$ (0.07)

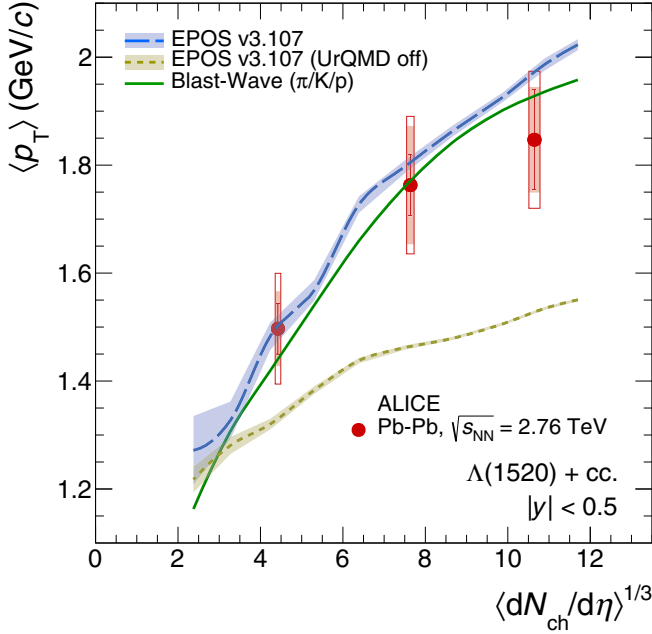


FIG. 3. $\langle p_T \rangle$ of $\Lambda(1520)$ as a function of $\langle dN_{ch}/d\eta \rangle^{1/3}$. Statistical and systematic uncertainties are shown as bars and boxes, respectively. The solid line shows the blast-wave predictions. The dashed lines show the predictions from EPOS3 with and without the hadronic phase (UrQMD off).

of the relevant hadronic cross sections in the transport phase. These observations highlight the relevance of the hadronic phase in the study of heavy-ion collisions and the importance of a microscopic description of the late hadronic interactions.

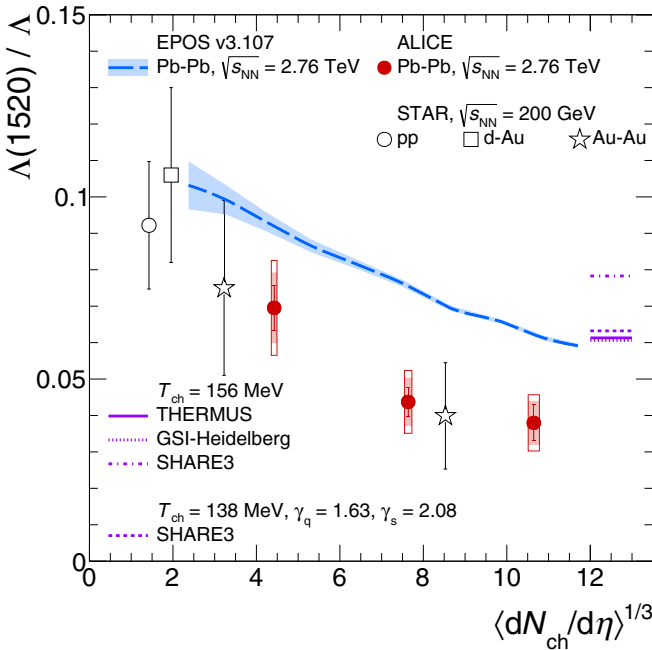


FIG. 4. p_T -integrated ratio of $\Lambda(1520)/\Lambda$ production as a function of $\langle dN_{ch}/d\eta \rangle^{1/3}$. Predictions from several SHMs and from EPOS3 are also shown.

IV. CONCLUSION

In conclusion, the first measurement of $\Lambda(1520)$ production in Pb-Pb collisions at $\sqrt{s_{NN}} = 2.76$ TeV at the LHC has been presented. The spectral shapes and $\langle p_T \rangle$ are consistent with the hydrodynamic evolution picture that describes pions, kaons, and protons, indicating that the $\Lambda(1520)$ experiences the same collective radial expansion, with a common transverse velocity which increases with collision centrality. The comparison of the $\langle p_T \rangle$ results to EPOS3 predictions highlights the relevance of the hadronic phase in the study of heavy-ion collisions and the importance of a microscopic description of the late hadronic interactions. The p_T -integrated ratio $\Lambda(1520)/\Lambda$ is suppressed in central Pb-Pb collisions with respect to peripheral Pb-Pb collisions (first such evidence in heavy-ion collisions) and is lower than the value predicted by statistical hadronisation models. The measurement adds further support to the formation of a dense hadronic phase in the latest stages of the evolution of the fireball created in high-energy heavy-ion collisions, lasting long enough to cause a significant reduction in the observable yield of short-lived resonances.

ACKNOWLEDGMENTS

The ALICE Collaboration would like to thank all its engineers and technicians for their invaluable contributions to the construction of the experiment and the CERN accelerator teams for the outstanding performance of the LHC complex. The ALICE Collaboration gratefully acknowledges the resources and support provided by all Grid centers and the Worldwide LHC Computing Grid (WLCG) Collaboration. The ALICE Collaboration acknowledges the following funding agencies for their support in building and running the ALICE detector: A. I. Alikhanyan National Science Laboratory (Yerevan Physics Institute) Foundation (ANSL), State Committee of Science and World Federation of Scientists (WFS), Armenia; Austrian Academy of Sciences and Nationalstiftung für Forschung, Technologie und Entwicklung, Austria; Ministry of Communications and High Technologies, National Nuclear Research Center, Azerbaijan; Conselho Nacional de Desenvolvimento Científico e Tecnológico (CNPq), Universidade Federal do Rio Grande do Sul (UFRGS), Financiadora de Estudos e Projetos (Finep) and Fundação de Amparo à Pesquisa do Estado de São Paulo (FAPESP), Brazil; Ministry of Science and Technology of China (MSTC), National Natural Science Foundation of China (NSFC), and Ministry of Education of China (MOEC), China; Ministry of Science and Education, Croatia; Ministry of Education, Youth, and Sports of the Czech Republic, Czech Republic; The Danish Council for Independent Research | Natural Sciences, the Carlsberg Foundation, and Danish National Research Foundation (DNRF), Denmark; Helsinki Institute of Physics (HIP), Finland; Commissariat à l’Energie Atomique (CEA), Institut National de Physique Nucléaire et de Physique des Particules (IN2P3), and Centre National de la Recherche Scientifique (CNRS), France; Bundesministerium für Bildung, Wissenschaft, Forschung, und Technologie (BMBF) and GSI Helmholtzzentrum für Schwerionenforschung GmbH,

Germany; General Secretariat for Research and Technology, Ministry of Education, Research, and Religions, Greece; National Research, Development, and Innovation Office, Hungary; Department of Atomic Energy Government of India (DAE), Department of Science and Technology, Government of India (DST), University Grants Commission, Government of India (UGC), and Council of Scientific and Industrial Research (CSIR), India; Indonesian Institute of Science, Indonesia; Centro Fermi - Museo Storico della Fisica e Centro Studi e Ricerche Enrico Fermi and Istituto Nazionale di Fisica Nucleare (INFN), Italy; Institute for Innovative Science and Technology, Nagasaki Institute of Applied Science (IIST), Japan Society for the Promotion of Science (JSPS) KAKENHI, and Japanese Ministry of Education, Culture, Sports, Science, and Technology (MEXT), Japan; Consejo Nacional de Ciencia (CONACYT) y Tecnología, through Fondo de Cooperación Internacional en Ciencia y Tecnología (FONCICYT) and Dirección General de Asuntos del Personal Académico (DGAPA), Mexico; Nederlandse Organisatie voor Wetenschappelijk Onderzoek (NWO), Netherlands; The Research Council of Norway, Norway; Commission on Science and Technology for Sustainable Development in the South (COMSATS), Pakistan; Pontificia Universidad Católica del Perú, Peru; Ministry of Science and Higher Education and National Science Centre, Poland; Korea Institute of Science and

Technology Information and National Research Foundation of Korea (NRF), Republic of Korea; Ministry of Education and Scientific Research, Institute of Atomic Physics, and Romanian National Agency for Science, Technology, and Innovation, Romania; Joint Institute for Nuclear Research (JINR), Ministry of Education and Science of the Russian Federation, and National Research Centre Kurchatov Institute, Russia; Ministry of Education, Science, Research, and Sport of the Slovak Republic, Slovakia; National Research Foundation of South Africa, South Africa; Centro de Aplicaciones Tecnológicas y Desarrollo Nuclear (CEADEN), Cubaenergía, Cuba and Centro de Investigaciones Energéticas, Medioambientales y Tecnológicas (CIEMAT), Spain; Swedish Research Council (VR) and Knut and Alice Wallenberg Foundation (KAW), Sweden; European Organization for Nuclear Research, Switzerland; National Science and Technology Development Agency (NSDTA), Suranaree University of Technology (SUT), and Office of the Higher Education Commission under NRU project of Thailand, Thailand; Turkish Atomic Energy Agency (TAEK), Turkey; National Academy of Sciences of Ukraine, Ukraine; Science and Technology Facilities Council (STFC), United Kingdom; and National Science Foundation of the United States of America (NSF) and United States Department of Energy, Office of Nuclear Physics (DOE NP), United States of America.

-
- [1] N. Cabibbo and G. Parisi, Exponential hadronic spectrum and quark liberation, *Phys. Lett. B* **59**, 67 (1975).
- [2] E. Laermann and O. Philipsen, The status of lattice QCD at finite temperature, *Ann. Rev. Nucl. Part. Sci.* **53**, 163 (2003).
- [3] B. Müller and J. L. Nagle, Results from the Relativistic Heavy Ion Collider, *Ann. Rev. Nucl. Part. Sci.* **56**, 93 (2006).
- [4] A. Andronic, P. Braun-Munzinger, and J. Stachel, Hadron production in central nucleus-nucleus collisions at chemical freeze-out, *Nucl. Phys. A* **772**, 167 (2006).
- [5] F. Becattini and R. Fries, The QCD confinement transition: Hadron formation, Landolt-Börnstein - Group I Elementary Particles, Nuclei and Atoms - Vol. 23 (Springer-Verlag, Berlin Heidelberg, 2010).
- [6] J. Cleymans and K. Redlich, Unified Description of Freezeout Parameters in Relativistic Heavy Ion Collisions, *Phys. Rev. Lett.* **81**, 5284 (1998).
- [7] A. Andronic, P. Braun-Munzinger, K. Redlich, and J. Stachel, The thermal model on the verge of the ultimate test: Particle production in Pb-Pb collisions at the LHC, *J. Phys. G* **38**, 124081 (2011).
- [8] C. Markert, R. Bellwied, and I. Vitev, Formation and decay of hadronic resonances in the QGP, *Phys. Lett. B* **669**, 92 (2008).
- [9] M. Bleicher and J. Aichelin, Strange resonance production: Probing chemical and thermal freezeout in relativistic heavy ion collisions, *Phys. Lett. B* **530**, 81 (2002).
- [10] B. Abelev *et al.* (ALICE Collaboration), $K^*(892)^0$ and $\phi(1020)$ production in Pb-Pb collisions at $\sqrt{s_{NN}} = 2.76$ TeV, *Phys. Rev. C* **91**, 024609 (2015).
- [11] A. G. Knospe, C. Markert, K. Werner, J. Steinheimer, and M. Bleicher, Hadronic resonance production and interaction in partonic and hadronic matter in the EPOS3 model with and without the hadronic afterburner UrQMD, *Phys. Rev. C* **93**, 014911 (2016).
- [12] K. Aamodt *et al.* (ALICE Collaboration), The ALICE experiment at the CERN LHC, *JINST* **3**, S08002 (2008).
- [13] B. I. Abelev *et al.* (STAR Collaboration), Strange Baryon Resonance Production in $\sqrt{s_{NN}} = 200$ GeV $p + p$ and Au+Au Collisions, *Phys. Rev. Lett.* **97**, 132301 (2006).
- [14] B. I. Abelev *et al.* (STAR Collaboration), Hadronic resonance production in $d+Au$ collisions at $\sqrt{s_{NN}} = 200$ GeV at RHIC, *Phys. Rev. C* **78**, 044906 (2008).
- [15] B. Abelev *et al.* (ALICE Collaboration), Performance of the ALICE Experiment at the CERN LHC, *Int. J. Mod. Phys. A* **29**, 1430044 (2014).
- [16] K. Aamodt *et al.* (ALICE Collaboration), Charged-Particle Multiplicity Density at Mid-Rapidity in Central Pb-Pb Collisions at $\sqrt{s_{NN}} = 2.76$ TeV, *Phys. Rev. Lett.* **105**, 252301 (2010).
- [17] K. Aamodt *et al.* (ALICE Collaboration), Centrality Dependence of the Charged-Particle Multiplicity Density at Mid-Rapidity in Pb-Pb Collisions at $\sqrt{s_{NN}} = 2.76$ TeV, *Phys. Rev. Lett.* **106**, 032301 (2011).
- [18] B. Abelev *et al.* (ALICE Collaboration), Centrality determination of Pb-Pb collisions at $\sqrt{s_{NN}} = 2.76$ TeV with ALICE, *Phys. Rev. C* **88**, 044909 (2013).
- [19] C. Patrignani, K. Agashe, G. Aielli, C. Amsler, M. Antonelli, D. M. Asner, H. Baer, Sw. Banerjee, R. M. Barnett, T. Basaglia *et al.*, Review of particle physics, *Chin. Phys. C* **40**, 100001 (2016).
- [20] D. L'Hote, About resonance signal extraction from multiparticle data: Combinatorics and event mixing methods, *Nucl. Instrum. Meth. A* **337**, 544 (1994).

- [21] X.-N. Wang and M. Gyulassy, HIJING: A Monte Carlo model for multiple jet production in pp , pA , and AA collisions, *Phys. Rev. D* **44**, 3501 (1991).
- [22] R. Brun, F. Bruyant, F. Carminati, S. Giani, M. Maire, A. McPherson, G. Patrick, and L. Urban, GEANT Detector Description and Simulation Tool [<http://cds.cern.ch/record/1082634>]
- [23] E. Schnedermann, J. Sollfrank, and U. W. Heinz, Thermal phenomenology of hadrons from 200-A/GeV S+S collisions, *Phys. Rev. C* **48**, 2462 (1993).
- [24] B. Abelev *et al.* (ALICE Collaboration), Centrality dependence of π , K, p production in Pb-Pb collisions at $\sqrt{s_{NN}} = 2.76$ TeV, *Phys. Rev. C* **88**, 044910 (2013).
- [25] S. A. Bass, M. Belkacem, M. Brandstetter, L. Bravina, C. Ernest, L. Gerland, M. Hofmann, S. Hofmann, J. Konopka, G. Mao *et al.*, Microscopic models for ultrarelativistic heavy ion collisions, *Prog. Part. Nucl. Phys.* **41**, 255 (1998).
- [26] M. Bleicher, E. Zabrodin, C. Spieles, S. A. Bass, C. Ernst, S. Soff, L. Bravina, M. Belkacem, H. Weber, H. Stöcker *et al.*, Relativistic hadron hadron collisions in the ultrarelativistic quantum molecular dynamics model, *J. Phys. G* **25**, 1859 (1999).
- [27] B. Abelev *et al.* (ALICE Collaboration), K_S^0 and Λ Production in Pb-Pb Collisions at $\sqrt{s_{NN}} = 2.76$ TeV, *Phys. Rev. Lett.* **111**, 222301 (2013).
- [28] K. Aamodt *et al.* (ALICE Collaboration), Two-pion Bose-Einstein correlations in central Pb-Pb collisions at $\sqrt{s_{NN}} = 2.76$ TeV, *Phys. Lett. B* **696**, 328 (2011).
- [29] S. Wheaton and J. Cleymans, Statistical-thermal model calculations using THERMUS, *J. Phys. G* **31**, S1069 (2005).
- [30] M. Petran, J. Letessier, J. Rafelski, and G. Torrieri, SHARE with CHARM, *Comput. Phys. Commun.* **185**, 2056 (2014).
- [31] M. Floris, Hadron yields and the phase diagram of strongly interacting matter, *Nucl. Phys. A* **931**, 103 (2014).
- [32] M. Petran, J. Letessier, V. Petraek, and J. Rafelski, Hadron production and quark-gluon plasma hadronization in Pb-Pb collisions at $\sqrt{s_{NN}} = 2.76$ TeV, *Phys. Rev. C* **88**, 034907 (2013).

S. Acharya,¹³⁸ D. Adamová,⁹⁴ J. Adolfsson,⁸¹ M. M. Aggarwal,⁹⁸ G. Aglieri Rinella,³⁶ M. Agnello,³³ N. Agrawal,⁴⁹ Z. Ahammed,¹³⁸ S. U. Ahn,⁷⁷ S. Aiola,¹⁴³ A. Akindinov,⁶⁵ M. Al-Turany,¹⁰⁴ S. N. Alam,¹³⁸ D. S. D. Albuquerque,¹²⁰ D. Aleksandrov,⁸⁸ B. Alessandro,⁵⁹ R. Alfaro Molina,⁷³ Y. Ali,¹⁶ A. Alici,^{11,54,29} A. Alkin,³ J. Alme,²⁴ T. Alt,⁷⁰ L. Altenkamper,²⁴ I. Altsybeev,¹³⁷ M. N. Anaam,⁷ C. Andrei,⁴⁸ D. Andreou,³⁶ H. A. Andrews,¹⁰⁸ A. Andronic,^{141,104} M. Angeletti,³⁶ V. Anguelov,¹⁰² C. Anson,¹⁷ T. Antičić,¹⁰⁵ F. Antinori,⁵⁷ P. Antonioli,⁵⁴ R. Anwar,¹²⁴ N. Apadula,⁸⁰ L. Aphecetche,¹¹² H. Appelshäuser,⁷⁰ S. Arceci,²⁹ R. Arnaldi,⁵⁹ O. W. Arnold,^{103,115} I. C. Arsene,²³ M. Arstrandok,¹⁰² B. Audurier,¹¹² A. Augustinus,³⁶ R. Averbeck,¹⁰⁴ M. D. Azmi,¹⁸ A. Badalà,⁵⁶ Y. W. Baek,^{61,42} S. Bagnasco,⁵⁹ R. Bailhache,⁷⁰ R. Bala,⁹⁹ A. Baldisseri,¹³⁴ M. Ball,⁴⁴ R. C. Baral,⁸⁶ A. M. Barbano,²⁸ R. Barbera,³⁰ F. Barile,⁵³ L. Barioglio,²⁸ G. G. Barnaföldi,¹⁴² L. S. Barnby,⁹³ V. Barret,¹³¹ P. Bartalini,⁷ K. Barth,³⁶ E. Bartsch,⁷⁰ N. Bastid,¹³¹ S. Basu,¹⁴⁰ G. Batigne,¹¹² B. Batyunya,⁷⁶ P. C. Batzing,²³ J. L. Bazo Alba,¹⁰⁹ I. G. Bearden,⁸⁹ H. Beck,¹⁰² C. Bedda,⁶⁴ N. K. Behera,⁶¹ I. Belikov,¹³³ F. Bellini,³⁶ H. Bello Martinez,² R. Bellwied,¹²⁴ L. G. E. Beltran,¹¹⁸ V. Belyaev,⁹² G. Bencedi,¹⁴² S. Beole,²⁸ A. Bercuci,⁴⁸ Y. Berdnikov,⁹⁶ D. Berenyi,¹⁴² R. A. Bertens,¹²⁷ D. Berzano,^{36,59} L. Betev,³⁶ P. P. Bhaduri,¹³⁸ A. Bhasin,⁹⁹ I. R. Bhat,⁴⁹ H. Bhatt,⁴⁹ B. Bhattacharjee,⁴³ J. Bhom,¹¹⁶ A. Bianchi,²⁸ L. Bianchi,¹²⁴ N. Bianchi,⁵² J. Bielčák,³⁹ J. Bielčiková,⁹⁴ A. Bilandzic,^{115,103} G. Biro,¹⁴² R. Biswas,⁴ S. Biswas,⁴ J. T. Blair,¹¹⁷ D. Blau,⁸⁸ C. Blume,⁷⁰ G. Boca,¹³⁵ F. Bock,³⁶ A. Bogdanov,⁹² L. Boldizsár,¹⁴² M. Bombara,⁴⁰ G. Bonomi,¹³⁶ M. Bonora,³⁶ H. Borel,¹³⁴ A. Borrisov,^{20,141} M. Borri,¹²⁶ E. Botta,²⁸ C. Bourjau,⁸⁹ L. Bratrud,⁷⁰ P. Braun-Munzinger,¹⁰⁴ M. Bregant,¹¹⁹ T. A. Broker,⁷⁰ M. Broz,³⁹ E. J. Brucken,⁴⁵ E. Bruna,⁵⁹ G. E. Bruno,^{36,35} D. Budnikov,¹⁰⁶ H. Buesching,⁷⁰ S. Bufalino,³³ P. Buhler,¹¹¹ P. Buncic,³⁶ O. Busch,^{130,a} Z. Buthelezi,⁷⁴ J. B. Butt,¹⁶ J. T. Buxton,¹⁹ J. Cabala,¹¹⁴ D. Caffarri,⁹⁰ H. Caines,¹⁴³ A. Caliva,¹⁰⁴ E. Calvo Villar,¹⁰⁹ R. S. Camacho,² P. Camerini,²⁷ A. A. Capon,¹¹¹ F. Carena,³⁶ W. Carena,³⁶ F. Carnesecchi,^{29,11} J. Castillo Castellanos,¹³⁴ A. J. Castro,¹²⁷ E. A. R. Casula,⁵⁵ C. Ceballos Sanchez,⁹ S. Chandra,¹³⁸ B. Chang,¹²⁵ W. Chang,⁷ S. Chapeland,³⁶ M. Chartier,¹²⁶ S. Chattopadhyay,¹³⁸ S. Chattopadhyay,¹⁰⁷ A. Chauvin,^{103,115} C. Cheshkov,¹³² B. Cheynis,¹³² V. Chibante Barroso,³⁶ D. D. Chinellato,¹²⁰ S. Cho,⁶¹ P. Chochula,³⁶ T. Chowdhury,¹³¹ P. Christakoglou,⁹⁰ C. H. Christensen,⁸⁹ P. Christiansen,⁸¹ T. Chujo,¹³⁰ S. U. Chung,²⁰ C. Cicalo,⁵⁵ L. Cifarelli,^{11,29} F. Cindolo,⁵⁴ J. Cleymans,¹²³ F. Colamaria,⁵³ D. Colella,^{66,36,53} A. Collu,⁸⁰ M. Colocci,²⁹ M. Concas,^{59,b} G. Conesa Balbastre,⁷⁹ Z. Conesa del Valle,⁶² J. G. Contreras,³⁹ T. M. Cormier,⁹⁵ Y. Corrales Morales,⁵⁹ P. Cortese,³⁴ M. R. Cosentino,¹²¹ F. Costa,³⁶ S. Costanza,¹³⁵ J. Crkovská,⁶² P. Crochet,¹³¹ E. Cuautle,⁷¹ L. Cunqueiro,^{141,95} T. Dahms,^{103,115} A. Dainese,⁵⁷ S. Dani,⁶⁷ M. C. Danisch,¹⁰² A. Danu,⁶⁹ D. Das,¹⁰⁷ I. Das,¹⁰⁷ S. Das,⁴ A. Dash,⁸⁶ S. Dash,⁴⁹ S. De,⁵⁰ A. De Caro,³² G. de Cataldo,⁵³ C. de Conti,¹¹⁹ J. de Cuveland,⁴¹ A. De Falco,²⁶ D. De Gruttola,^{11,32} N. De Marco,⁵⁹ S. De Pasquale,³² R. D. De Souza,¹²⁰ H. F. Degenhardt,¹¹⁹ A. Deisting,^{104,102} A. Deloff,⁸⁵ S. Delsanto,²⁸ C. Deplano,⁹⁰ P. Dhankher,⁴⁹ D. Di Bari,³⁵ A. Di Mauro,³⁶ B. Di Ruzza,⁵⁷ R. A. Diaz,⁹ T. Dietel,¹²³ P. Dillenseger,⁷⁰ Y. Ding,⁷ R. Divià,³⁶ Ø. Djuvsland,²⁴ A. Dobrin,³⁶ D. Domenicis Gimenez,¹¹⁹ B. Dönigus,⁷⁰ O. Dordic,²³ L. V. R. Doremalen,⁶⁴ A. K. Dubey,¹³⁸ A. Dubla,¹⁰⁴ L. Ducroux,¹³² S. Dudi,⁹⁸ A. K. Duggal,⁹⁸ M. Dukhishyam,⁸⁶ P. Dupieux,¹³¹ R. J. Ehlers,¹⁴³ D. Elia,⁵³ E. Endress,¹⁰⁹ H. Engel,⁷⁵ E. Epple,¹⁴³ B. Erazmus,¹¹² F. Erhardt,⁹⁷ M. R. Ersdal,²⁴ B. Espagnon,⁶² G. Eulisse,³⁶ J. Eum,²⁰ D. Evans,¹⁰⁸ S. Evdokimov,⁹¹ L. Fabbietti,^{103,115} M. Faggin,³¹ J. Faivre,⁷⁹ A. Fantoni,⁵² M. Fasel,⁹⁵ L. Feldkamp,¹⁴¹ A. Feliciello,⁵⁹ G. Feofilov,¹³⁷ A. Fernández Téllez,² A. Ferretti,²⁸ A. Festanti,^{31,36} V. J. G. Feuillard,¹⁰² J. Figiel,¹¹⁶ M. A. S. Figueredo,¹¹⁹ S. Filchagin,¹⁰⁶ D. Finogeev,⁶³ F. M. Fionda,²⁴ G. Fiorenza,⁵³ F. Flor,¹²⁴ M. Floris,³⁶ S. Foertsch,⁷⁴ P. Foka,¹⁰⁴ S. Fokin,⁸⁸ E. Fragiacomo,⁶⁰ A. Francescon,³⁶ A. Francisco,¹¹²

A. Rehman,²⁴ P. Reichelt,⁷⁰ F. Reidt,³⁶ X. Ren,⁷ R. Renfordt,⁷⁰ A. Reshetin,⁶³ J.-P. Revol,¹¹ K. Reygers,¹⁰² V. Riabov,⁹⁶ T. Richert,^{64,81} M. Richter,²³ P. Riedler,³⁶ W. Riegler,³⁶ F. Riggi,³⁰ C. Ristea,⁶⁹ S. P. Rode,⁵⁰ M. Rodríguez Cahuantzi,² K. Røed,²³ R. Rogalev,⁹¹ E. Rogochaya,⁷⁶ D. Rohr,³⁶ D. Röhrich,²⁴ P. S. Rokita,¹³⁹ F. Ronchetti,⁵² E. D. Rosas,⁷¹ K. Roslon,¹³⁹ P. Rosnet,¹³¹ A. Rossi,³¹ A. Rotondi,¹³⁵ F. Roukoutakis,⁸⁴ C. Roy,¹³³ P. Roy,¹⁰⁷ O. V. Rueda,⁷¹ R. Rui,²⁷ B. Rumyantsev,⁷⁶ A. Rustamov,⁸⁷ E. Ryabinkin,⁸⁸ Y. Ryabov,⁹⁶ A. Rybicki,¹¹⁶ S. Saarinen,⁴⁵ S. Sadhu,¹³⁸ S. Sadovsky,⁹¹ K. Šafařík,³⁶ S. K. Saha,¹³⁸ B. Sahoo,⁴⁹ P. Sahoo,⁵⁰ R. Sahoo,⁵⁰ S. Sahoo,⁵⁷ P. K. Sahu,⁶⁷ J. Saini,¹³⁸ S. Sakai,¹³⁰ M. A. Saleh,¹⁴⁰ S. Sambyal,⁹⁹ V. Samsonov,^{96,92} A. Sandoval,⁷³ A. Sarkar,⁷⁴ D. Sarkar,¹³⁸ N. Sarkar,¹³⁸ P. Sarma,⁴³ M. H. P. Sas,⁶⁴ E. Scapparone,⁵⁴ F. Scarlassara,³¹ B. Schaefer,⁹⁵ H. S. Scheid,⁷⁰ C. Schiaua,⁴⁸ R. Schicker,¹⁰² C. Schmidt,¹⁰⁴ H. R. Schmidt,¹⁰¹ M. O. Schmidt,¹⁰² M. Schmidt,¹⁰¹ N. V. Schmidt,^{95,70} J. Schukraft,³⁶ Y. Schutz,^{36,133} K. Schwarz,¹⁰⁴ K. Schweda,¹⁰⁴ G. Scioli,²⁹ E. Scomparin,⁵⁹ M. Šeščík,⁴⁰ J. E. Seger,¹⁷ Y. Sekiguchi,¹²⁹ D. Sekihata,⁴⁶ I. Selyuzhenkov,^{104,92} K. Senosi,⁷⁴ S. Senyukov,¹³³ E. Serradilla,⁷³ P. Sett,⁴⁹ A. Sevcenco,⁶⁹ A. Shabanov,⁶³ A. Shabetai,¹¹² R. Shahoyan,³⁶ W. Shaikh,¹⁰⁷ A. Shangaraev,⁹¹ A. Sharma,⁹⁸ A. Sharma,⁹⁹ M. Sharma,⁹⁹ N. Sharma,⁹⁸ A. I. Sheikh,¹³⁸ K. Shigaki,⁴⁶ M. Shimomura,⁸³ S. Shirinkin,⁶⁵ Q. Shou,^{7,110} K. Shtejer,²⁸ Y. Sibiriak,⁸⁸ S. Siddhanta,⁵⁵ K. M. Sielewicz,³⁶ T. Siemiarczuk,⁸⁵ D. Silvermyr,⁸¹ G. Simatovic,⁹⁰ G. Simonetti,^{36,103} R. Singaraju,¹³⁸ R. Singh,⁸⁶ R. Singh,⁹⁹ V. Singhal,¹³⁸ T. Sinha,¹⁰⁷ B. Sitar,¹⁵ M. Sitta,³⁴ T. B. Skaali,²³ M. Slupecki,¹²⁵ N. Smirnov,¹⁴³ R. J. M. Snellings,⁶⁴ T. W. Snellman,¹²⁵ J. Song,²⁰ F. Soramel,³¹ S. Sorensen,¹²⁷ F. Sozzi,¹⁰⁴ I. Sputowska,¹¹⁶ J. Stachel,¹⁰² I. Stan,⁶⁹ P. Stankus,⁹⁵ E. Stenlund,⁸¹ D. Stocco,¹¹² M. M. Storetvedt,³⁸ P. Strmen,¹⁵ A. A. P. Suaide,¹¹⁹ T. Sugitate,⁴⁶ C. Suire,⁶² M. Suleymanov,¹⁶ M. Suljic,^{36,27} R. Sultanov,⁶⁵ M. Šumbera,⁹⁴ S. Sumowidagdo,⁵¹ K. Suzuki,¹¹¹ S. Swain,⁶⁷ A. Szabo,¹⁵ I. Szarka,¹⁵ U. Tabassam,¹⁶ J. Takahashi,¹²⁰ G. J. Tambave,²⁴ N. Tanaka,¹⁵⁰ M. Tarhini,¹¹² M. Tariq,¹⁸ M. G. Tarzila,⁴⁸ A. Tauro,³⁶ G. Tejada Muñoz,² A. Telesca,³⁶ C. Terrevoli,³¹ B. Teyssier,¹³² D. Thakur,⁵⁰ S. Thakur,¹³⁸ D. Thomas,¹¹⁷ F. Thoresen,⁸⁹ R. Tieulent,¹³² A. Tikhonov,⁶³ A. R. Timmins,¹²⁴ A. Toia,⁷⁰ N. Topilskaya,⁶³ M. Toppi,⁵² F. Torales-Acosta,²² S. R. Torres,¹¹⁸ S. Tripathy,⁵⁰ S. Trogolo,²⁸ G. Trombetta,³⁵ L. Tropp,⁴⁰ V. Trubnikov,³ W. H. Trzaska,¹²⁵ T. P. Trzcinski,¹³⁹ B. A. Trzeciak,⁶⁴ T. Tsuji,¹²⁹ A. Tumkin,¹⁰⁶ R. Turrisi,⁵⁷ T. S. Tveter,²³ K. Ullaland,²⁴ E. N. Umaka,¹²⁴ A. Uras,¹³² G. L. Usai,²⁶ A. Utrobicic,⁹⁷ M. Vala,¹¹⁴ J. W. Van Hoorne,³⁶ M. van Leeuwen,⁶⁴ P. Vande Vyvre,³⁶ D. Varga,¹⁴² A. Vargas,² M. Vargyas,¹²⁵ R. Varma,⁴⁹ M. Vasileiou,⁸⁴ A. Vasiliev,⁸⁸ A. Vauthier,⁷⁹ O. Vázquez Doce,^{103,115} V. Vechernin,¹³⁷ A. M. Veen,⁶⁴ E. Vercellin,²⁸ S. Vergara Limón,² L. Vermunt,⁶⁴ R. Vernet,⁸ R. Vértesi,¹⁴² L. Vickovic,³⁷ J. Viinikainen,¹²⁵ Z. Vilakazi,¹²⁸ O. Villalobos Baillie,¹⁰⁸ A. Villatoro Tello,² A. Vinogradov,⁸⁸ T. Virgili,³² V. Vislavicius,^{89,81} A. V. Vodopyanov,⁷⁶ M. A. Völkl,¹⁰¹ K. Voloshin,⁶⁵ S. A. Voloshin,¹⁴⁰ G. Volpe,³⁵ B. von Haller,³⁶ I. Vorobyev,^{115,103} D. Voscek,¹¹⁴ D. Vranic,^{104,36} J. Vrláková,⁴⁰ B. Wagner,²⁴ H. Wang,⁶⁴ M. Wang,⁷ Y. Watanabe,¹³⁰ M. Weber,¹¹¹ S. G. Weber,¹⁰⁴ A. Wegrzynek,³⁶ D. F. Weiser,¹⁰² S. C. Wenzel,³⁶ J. P. Wessels,¹⁴¹ U. Westerhoff,¹⁴¹ A. M. Whitehead,¹²³ J. Wiechula,⁷⁰ J. Wikne,²³ G. Wilk,⁸⁵ J. Wilkinson,⁵⁴ G. A. Willems,^{141,36} M. C. S. Williams,⁵⁴ E. Willsher,¹⁰⁸ B. Windelband,¹⁰² W. E. Witt,¹²⁷ R. Xu,⁷ S. Yalcin,⁷⁸ K. Yamakawa,⁴⁶ S. Yano,⁴⁶ Z. Yin,⁷ H. Yokoyama,^{79,130} I.-K. Yoo,²⁰ J. H. Yoon,⁶¹ V. Yurchenko,³ V. Zaccolo,⁵⁹ A. Zaman,¹⁶ C. Zampolli,³⁶ H. J. C. Zanoli,¹¹⁹ N. Zardoshti,¹⁰⁸ A. Zarochentsev,¹³⁷ P. Závada,⁶⁸ N. Zaviyalov,¹⁰⁶ H. Zbroszczyk,¹³⁹ M. Zhalov,⁹⁶ X. Zhang,⁷ Y. Zhang,⁷ Z. Zhang,^{7,131} C. Zhao,²³ V. Zhrebchevskii,¹³⁷ N. Zhigareva,⁶⁵ D. Zhou,⁷ Y. Zhou,⁸⁹ Z. Zhou,²⁴ H. Zhu,⁷ J. Zhu,⁷ Y. Zhu,⁷ A. Zichichi,^{29,11} M. B. Zimmermann,³⁶ G. Zinovjev,³ J. Zmeskal,¹¹¹ and S. Zou⁷

(ALICE Collaboration)

¹A. I. Alikhanyan National Science Laboratory (Yerevan Physics Institute) Foundation, Yerevan, Armenia

²Benemérita Universidad Autónoma de Puebla, Puebla, Mexico

³Bogolyubov Institute for Theoretical Physics, National Academy of Sciences of Ukraine, Kiev, Ukraine

⁴Bose Institute, Department of Physics and Centre for Astroparticle Physics and Space Science (CAPSS), Kolkata, India

⁵Budker Institute for Nuclear Physics, Novosibirsk, Russia

⁶California Polytechnic State University, San Luis Obispo, California, USA

⁷Central China Normal University, Wuhan, China

⁸Centre de Calcul de l'IN2P3, Villeurbanne, Lyon, France

⁹Centro de Aplicaciones Tecnológicas y Desarrollo Nuclear (CEADEN), Havana, Cuba

¹⁰Centro de Investigación y de Estudios Avanzados (CINVESTAV), Mexico City and Mérida, Mexico

¹¹Centro Fermi - Museo Storico della Fisica e Centro Studi e Ricerche "Enrico Fermi," Rome, Italy

¹²Chicago State University, Chicago, Illinois, USA

¹³China Institute of Atomic Energy, Beijing, China

¹⁴Chonbuk National University, Jeonju, Republic of Korea

¹⁵Comenius University Bratislava, Faculty of Mathematics, Physics and Informatics, Bratislava, Slovakia

¹⁶COMSATS Institute of Information Technology (CIIT), Islamabad, Pakistan

¹⁷Creighton University, Omaha, Nebraska, USA

¹⁸Department of Physics, Aligarh Muslim University, Aligarh, India

¹⁹Department of Physics, Ohio State University, Columbus, Ohio, United States

²⁰Department of Physics, Pusan National University, Pusan, Republic of Korea

- ²¹Department of Physics, Sejong University, Seoul, Republic of Korea
²²Department of Physics, University of California, Berkeley, California, USA
²³Department of Physics, University of Oslo, Oslo, Norway
²⁴Department of Physics and Technology, University of Bergen, Bergen, Norway
²⁵Dipartimento di Fisica dell'Università 'La Sapienza' and Sezione INFN, Rome, Italy
²⁶Dipartimento di Fisica dell'Università and Sezione INFN, Cagliari, Italy
²⁷Dipartimento di Fisica dell'Università and Sezione INFN, Trieste, Italy
²⁸Dipartimento di Fisica dell'Università and Sezione INFN, Turin, Italy
²⁹Dipartimento di Fisica e Astronomia dell'Università and Sezione INFN, Bologna, Italy
³⁰Dipartimento di Fisica e Astronomia dell'Università and Sezione INFN, Catania, Italy
³¹Dipartimento di Fisica e Astronomia dell'Università and Sezione INFN, Padova, Italy
³²Dipartimento di Fisica 'E.R. Caianiello' dell'Università and Gruppo Collegato INFN, Salerno, Italy
³³Dipartimento DISAT del Politecnico and Sezione INFN, Turin, Italy
³⁴Dipartimento di Scienze e Innovazione Tecnologica dell'Università del Piemonte Orientale and INFN Sezione di Torino, Alessandria, Italy
³⁵Dipartimento Interateneo di Fisica "M. Merlin" and Sezione INFN, Bari, Italy
³⁶European Organization for Nuclear Research (CERN), Geneva, Switzerland
³⁷Faculty of Electrical Engineering, Mechanical Engineering and Naval Architecture, University of Split, Split, Croatia
³⁸Faculty of Engineering and Science, Western Norway University of Applied Sciences, Bergen, Norway
³⁹Faculty of Nuclear Sciences and Physical Engineering, Czech Technical University in Prague, Prague, Czech Republic
⁴⁰Faculty of Science, P. J. Šafárik University, Košice, Slovakia
⁴¹Frankfurt Institute for Advanced Studies, Johann Wolfgang Goethe-Universität Frankfurt, Frankfurt, Germany
⁴²Gangneung-Wonju National University, Gangneung, Republic of Korea
⁴³Gauhati University, Department of Physics, Guwahati, India
⁴⁴Helmholtz-Institut für Strahlen- und Kernphysik, Rheinische Friedrich-Wilhelms-Universität Bonn, Bonn, Germany
⁴⁵Helsinki Institute of Physics (HIP), Helsinki, Finland
⁴⁶Hiroshima University, Hiroshima, Japan
⁴⁷Hochschule Worms, Zentrum für Technologietransfer und Telekommunikation (ZTT), Worms, Germany
⁴⁸Horia Hulubei National Institute of Physics and Nuclear Engineering, Bucharest, Romania
⁴⁹Indian Institute of Technology Bombay (IIT), Mumbai, India
⁵⁰Indian Institute of Technology Indore, Indore, India
⁵¹Indonesian Institute of Sciences, Jakarta, Indonesia
⁵²INFN, Laboratori Nazionali di Frascati, Frascati, Italy
⁵³INFN, Sezione di Bari, Bari, Italy
⁵⁴INFN, Sezione di Bologna, Bologna, Italy
⁵⁵INFN, Sezione di Cagliari, Cagliari, Italy
⁵⁶INFN, Sezione di Catania, Catania, Italy
⁵⁷INFN, Sezione di Padova, Padova, Italy
⁵⁸INFN, Sezione di Roma, Rome, Italy
⁵⁹INFN, Sezione di Torino, Turin, Italy
⁶⁰INFN, Sezione di Trieste, Trieste, Italy
⁶¹Inha University, Incheon, Republic of Korea
⁶²Institut de Physique Nucléaire d'Orsay (IPNO), Institut National de Physique Nucléaire et de Physique des Particules (IN2P3/CNRS), Université de Paris-Sud, Université Paris-Saclay, Orsay, France
⁶³Institute for Nuclear Research, Academy of Sciences, Moscow, Russia
⁶⁴Institute for Subatomic Physics, Utrecht University/Nikhef, Utrecht, Netherlands
⁶⁵Institute for Theoretical and Experimental Physics, Moscow, Russia
⁶⁶Institute of Experimental Physics, Slovak Academy of Sciences, Košice, Slovakia
⁶⁷Institute of Physics, Bhubaneswar, India
⁶⁸Institute of Physics of the Czech Academy of Sciences, Prague, Czech Republic
⁶⁹Institute of Space Science (ISS), Bucharest, Romania
⁷⁰Institut für Kernphysik, Johann Wolfgang Goethe-Universität Frankfurt, Frankfurt, Germany
⁷¹Instituto de Ciencias Nucleares, Universidad Nacional Autónoma de México, Mexico City, Mexico
⁷²Instituto de Física, Universidade Federal do Rio Grande do Sul (UFRGS), Porto Alegre, Brazil
⁷³Instituto de Física, Universidad Nacional Autónoma de México, Mexico City, Mexico
⁷⁴iThemba LABS, National Research Foundation, Somerset West, South Africa
⁷⁵Johann-Wolfgang-Goethe Universität Frankfurt Institut für Informatik, Fachbereich Informatik und Mathematik, Frankfurt, Germany
⁷⁶Joint Institute for Nuclear Research (JINR), Dubna, Russia
⁷⁷Korea Institute of Science and Technology Information, Daejeon, Republic of Korea
⁷⁸KTO Karatay University, Konya, Turkey

- ⁷⁹Laboratoire de Physique Subatomique et de Cosmologie, Université Grenoble-Alpes, CNRS-IN2P3, Grenoble, France
- ⁸⁰Lawrence Berkeley National Laboratory, Berkeley, California, USA
- ⁸¹Lund University Department of Physics, Division of Particle Physics, Lund, Sweden
- ⁸²Nagasaki Institute of Applied Science, Nagasaki, Japan
- ⁸³Nara Women's University (NWU), Nara, Japan
- ⁸⁴National and Kapodistrian University of Athens, School of Science, Department of Physics, Athens, Greece
- ⁸⁵National Centre for Nuclear Research, Warsaw, Poland
- ⁸⁶National Institute of Science Education and Research, HBNI, Jatni, India
- ⁸⁷National Nuclear Research Center, Baku, Azerbaijan
- ⁸⁸National Research Centre Kurchatov Institute, Moscow, Russia
- ⁸⁹Niels Bohr Institute, University of Copenhagen, Copenhagen, Denmark
- ⁹⁰Nikhef, National institute for subatomic physics, Amsterdam, Netherlands
- ⁹¹NRC Kurchatov Institute IHEP, Protvino, Russia
- ⁹²NRNU Moscow Engineering Physics Institute, Moscow, Russia
- ⁹³Nuclear Physics Group, STFC Daresbury Laboratory, Daresbury, United Kingdom
- ⁹⁴Nuclear Physics Institute of the Czech Academy of Sciences, Řež u Prahy, Czech Republic
- ⁹⁵Oak Ridge National Laboratory, Oak Ridge, Tennessee, USA
- ⁹⁶Petersburg Nuclear Physics Institute, Gatchina, Russia
- ⁹⁷Physics Department, Faculty of science, University of Zagreb, Zagreb, Croatia
- ⁹⁸Physics Department, Panjab University, Chandigarh, India
- ⁹⁹Physics Department, University of Jammu, Jammu, India
- ¹⁰⁰Physics Department, University of Rajasthan, Jaipur, India
- ¹⁰¹Physikalisches Institut, Eberhard-Karls-Universität Tübingen, Tübingen, Germany
- ¹⁰²Physikalisches Institut, Ruprecht-Karls-Universität Heidelberg, Heidelberg, Germany
- ¹⁰³Physik Department, Technische Universität München, Munich, Germany
- ¹⁰⁴Research Division and ExtreMe Matter Institute EMMI, GSI Helmholtzzentrum für Schwerionenforschung GmbH, Darmstadt, Germany
- ¹⁰⁵Rudjer Bošković Institute, Zagreb, Croatia
- ¹⁰⁶Russian Federal Nuclear Center (VNIIEF), Sarov, Russia
- ¹⁰⁷Saha Institute of Nuclear Physics, Kolkata, India
- ¹⁰⁸School of Physics and Astronomy, University of Birmingham, Birmingham, United Kingdom
- ¹⁰⁹Sección Física, Departamento de Ciencias, Pontificia Universidad Católica del Perú, Lima, Peru
- ¹¹⁰Shanghai Institute of Applied Physics, Shanghai, China
- ¹¹¹Stefan Meyer Institut für Subatomare Physik (SMI), Vienna, Austria
- ¹¹²SUBATECH, IMT Atlantique, Université de Nantes, CNRS-IN2P3, Nantes, France
- ¹¹³Suranaree University of Technology, Nakhon Ratchasima, Thailand
- ¹¹⁴Technical University of Košice, Košice, Slovakia
- ¹¹⁵Technische Universität München, Excellence Cluster "Universe," Munich, Germany
- ¹¹⁶The Henryk Niewodniczański Institute of Nuclear Physics, Polish Academy of Sciences, Cracow, Poland
- ¹¹⁷The University of Texas at Austin, Austin, Texas, USA
- ¹¹⁸Universidad Autónoma de Sinaloa, Culiacán, Mexico
- ¹¹⁹Universidade de São Paulo (USP), São Paulo, Brazil
- ¹²⁰Universidade Estadual de Campinas (UNICAMP), Campinas, Brazil
- ¹²¹Universidade Federal do ABC, Santo Andre, Brazil
- ¹²²University College of Southeast Norway, Tonsberg, Norway
- ¹²³University of Cape Town, Cape Town, South Africa
- ¹²⁴University of Houston, Houston, Texas, USA
- ¹²⁵University of Jyväskylä, Jyväskylä, Finland
- ¹²⁶University of Liverpool, Department of Physics, Oliver Lodge Laboratory, Liverpool, United Kingdom
- ¹²⁷University of Tennessee, Knoxville, Tennessee, USA
- ¹²⁸University of the Witwatersrand, Johannesburg, South Africa
- ¹²⁹University of Tokyo, Tokyo, Japan
- ¹³⁰University of Tsukuba, Tsukuba, Japan
- ¹³¹Université Clermont Auvergne, CNRS/IN2P3, LPC, Clermont-Ferrand, France
- ¹³²Université de Lyon, Université Lyon 1, CNRS/IN2P3, IPN-Lyon, Villeurbanne, Lyon, France
- ¹³³Université de Strasbourg, CNRS, IPHC UMR 7178, F-67000 Strasbourg, France, Strasbourg, France
- ¹³⁴Université Paris-Saclay Centre d'Études de Saclay (CEA), IRFU, Department de Physique Nucléaire (DPhN), Saclay, France
- ¹³⁵Università degli Studi di Pavia, Pavia, Italy
- ¹³⁶Università di Brescia, Brescia, Italy
- ¹³⁷V. Fock Institute for Physics, St. Petersburg State University, St. Petersburg, Russia

¹³⁸*Variable Energy Cyclotron Centre, Kolkata, India*

¹³⁹*Warsaw University of Technology, Warsaw, Poland*

¹⁴⁰*Wayne State University, Detroit, Michigan, USA*

¹⁴¹*Westfälische Wilhelms-Universität Münster, Institut für Kernphysik, Münster, Germany*

¹⁴²*Wigner Research Centre for Physics, Hungarian Academy of Sciences, Budapest, Hungary*

¹⁴³*Yale University, New Haven, Connecticut, USA*

¹⁴⁴*Yonsei University, Seoul, Republic of Korea*

^aDeceased.

^bPresent address: Dipartimento DET del Politecnico di Torino, Turin, Italy.

^cPresent address: M.V. Lomonosov Moscow State University, D.V. Skobeltsyn Institute of Nuclear, Physics, Moscow, Russia.

^dPresent address: Department of Applied Physics, Aligarh Muslim University, Aligarh, India.

^ePresent address: Institute of Theoretical Physics, University of Wrocław, Poland.